Regular Article

Analytical results for one-electron Rydberg quasimolecules in a high-frequency laser field

Nikolay Kryukov[1] and Eugene Oks[2,a]

[1] Universidad Nacional Autónoma de México, Av. Universidad 3000, col. Ciudad Universitaria, del. Coyoacán, México, DF 04510, Mexico

[2] Physics Department, 380 Duncan Drive, Auburn University, Auburn, AL 36849, USA

Abstract. The detailed description of electron terms in the field of two stationary Coulomb centers of charges Z and Z' separated by a distance R is one of the most fundamental problems in quantum mechanics. When the charges Z and Z' approach each other and share the only one electron that they have, they form a quasimolecule. Such quasimolecules are encountered in various kinds of plasmas and play an important role in theoretical and experimental studies of charge exchange. When the electron is in a highly-excited state, it is a one-electron Rydberg quasimolecule (OERQ). There are extensive analytical studies of the OERQ by the methods of classical mechanics (which are appropriate for Rydberg states). In one of our previous papers we studied the OERQ subjected to a laser field in the situation where the laser frequency was much smaller than the highest frequency of the unperturbed system. In the present paper we consider the situation where the OERQ is subjected to a laser field whose frequency is much greater than the highest frequency of the unperturbed system. For obtaining analytical results we use a generalization of the method of effective potentials. We show that as the amplitude of the laser field increases, in the case of the linearly-polarized laser field, the structure of the energy terms becomes more complex. Moreover the number of the energy terms increases in this case. We also calculated analytically the shift of the radiation frequency of OERQ caused by the laser field. As the amplitude of the laser field increases, so does the shift. The radiation frequency is shifted to the blue in the case of the linearly-polarized laser field, and to the red in the case of the circularly-polarized laser field. For a known amplitude of the laser field, by measuring the relative shift of the radiation frequency it should be possible to determine experimentally the distance of the orbital plane of the electron from the nucleus of the smaller nuclear charge.

1 Introduction

The detailed description of electron terms in the field of two stationary Coulomb centers (TCC) of charges Z and Z' separated by a distance R is one of the most fundamental problems in quantum mechanics. It presents fascinating atomic physics: the terms can have crossings and quasicrossings. On the one hand, the well-known Neumann-Wigner general theorem on the impossibility of crossing of terms of the same symmetry [1] is invalidated for the TCC problem of $Z' \neq Z$ (see e.g., paper [2]) – so the terms can cross. On the other hand when two potential wells (each corresponding to separated Z- and Z'-centers) have states Ψ and Ψ' of the same energies $E = E'$, of the same magnetic quantum numbers $m = m'$, and of the same radial elliptical quantum numbers $k = k'$, a quasicrossing of the terms occurs [3–5]. Then the electron has a much larger (by several orders of magnitude) probability

of tunneling from one well to the other (what constitutes charge exchange) compared to the absence of the quasicrossing.

In plasma spectroscopy a quasicrossing of the TCC terms, by facilitating charge exchange, can result in local dips in the spectral line profile emitted by a Z-ion from a plasma consisting of both Z- and Z'-ions – see e.g., theoretical and experimental papers [6–11]. In particular this allows one to determine rates of charge exchange between multicharged ions – the reference data almost inaccessible by other experimental methods [11].

When the charges Z and Z' approach each other and share the only one electron that they have, they form a quasimolecule. When the electron is in a highly-excited state the system can be described as a one-electron Rydberg quasimolecule (OERQ). There are extensive analytical studies of the OERQ by the methods of classical mechanics (which are appropriate for Rydberg states) [12–20] – see also review [21] and book [22] Chapter 3. In particular the following papers were devoted to studies of

---

a e-mail: goks@physics.auburn.edu

the OERQ in various external fields: namely in a static magnetic field [15], in a static electric field [16,17,19], and in a laser field [20]. Specifically in our previous paper [20] we analyzed the situation where the laser frequency was much smaller than the highest frequency of the unperturbed system.

In the present paper we consider the situation where the OERQ is subjected to a linearly-polarized or a circularly-polarized laser field whose frequency is much greater than the highest frequency of the unperturbed system. For obtaining analytical results we use a generalization of the method of effective potentials [23] (see also book [24], Appendix A). We show that as the amplitude of the linearly-polarized laser field increases the structure of the energy terms becomes more and more complex, and the number of the energy terms increases.

We also show that the laser field causes the blue or red shift of the radiation frequency of OERQ depending on whether the laser field is linearly- or circularly-polarized. The experimental determination of this shift would enable finding out the distance of the orbital plane of the electron from the nucleus of the smaller nuclear charge.

2 Analytical results

2.1 Linear polarization

We consider a TCC system with the charge Z placed at the origin and the Oz axis is directed at the charge Z', which is at $z = R$. Atomic units ($\hbar = e = m_e = 1$) are used throughout this article. The system is subjected to a high-frequency linearly-polarized laser field of amplitude F and frequency ω, the laser field being directed along the internuclear axis. It is well-known that the interaction of the laser field with Rydberg states can be correctly described classically (without engaging c-numbers describing the coherent quantum laser field). Therefore the semi-classical Hamiltonian for the electron in this configuration can be represented in the form

$$H = H_0 + zF\cos\omega t, H_0 = \frac{1}{2}\left(p_z^2 + p_\rho^2 + \frac{p_\varphi^2}{\rho^2}\right) - \frac{Z}{r} - \frac{Z'}{r'} \tag{1}$$

where $r = (\rho^2 + z^2)^{1/2}$ is the distance from the electron to the nucleus Z, $r' = (\rho^2 + (R-z)^2)^{1/2}$ is the distance from the electron to the nucleus Z', and (ρ, φ, z) are the cylindrical coordinates positioned in such a way that the nuclei Z and Z' are on the z-axis at $z = 0$ and $z = R$ accordingly. Due to φ-symmetry, φ is a cyclic coordinate and its corresponding momentum is conserved:

$$p_\varphi = \rho^2 \frac{d\varphi}{dt} = L. \tag{2}$$

For the systems in a high-frequency field, whose frequency is much greater than the highest frequency of the unperturbed system, it is appropriate to use the formalism of effective potentials [23,25,26]. As a result, the Hamiltonian

acquires a time-independent term. The zeroth-order effective potential,

$$U_0 = \frac{1}{4\omega^2}[V, [V, H_0]] = \frac{F^2}{4\omega^2} \tag{3}$$

where $V = zF$ and $[P, Q]$ are the Poisson brackets, is a coordinate-independent energy shift that does not affect the dynamics of the system. The first non-vanishing effect on the dynamics of the system originates from the first-order effective potential

$$U_1 = \frac{1}{4\omega^4}[[V, H_0], [[V, H_0], H_0]]$$
$$= \frac{F^2}{4\omega^4}\left(Z\frac{\rho^2 - 2z^2}{(\rho^2 + z^2)^{5/2}} + Z'\frac{\rho^2 - 2(R-z)^2}{\left(\rho^2 + (R-z)^2\right)^{5/2}}\right) \tag{4}$$

and the Hamiltonian of the electron in the high-frequency field is

$$H = \frac{1}{2}\left(p_z^2 + p_\rho^2\right) + \frac{L^2}{2\rho^2} - \frac{Z}{\sqrt{\rho^2 + z^2}} - \frac{Z'}{\sqrt{\rho^2 + (R-z)^2}} + U_1 \tag{5}$$

where U_1 is given by (4). The electron is considered to be in a circular state[1]. Therefore $p_z = p_\rho = 0$, and thus, its energy can be represented in the form

$$E = \frac{L^2}{2\rho^2} - \frac{Z}{\sqrt{\rho^2 + z^2}} - \frac{Z'}{\sqrt{\rho^2 + (R-z)^2}}$$
$$+ \frac{F^2}{4\omega^4}\left(Z\frac{\rho^2 - 2z^2}{(\rho^2 + z^2)^{5/2}} + Z'\frac{\rho^2 - 2(R-z)^2}{\left(\rho^2 + (R-z)^2\right)^{5/2}}\right). \tag{6}$$

Using the scaled quantities

$$w = \frac{z}{R}, v = \frac{\rho}{R}, \varepsilon = -\frac{R}{Z}E, b = \frac{Z'}{Z}, \ell = \frac{L}{\sqrt{ZR}},$$
$$r = \frac{Z}{L^2}R, \theta = \frac{F}{\omega^2 R} \tag{7}$$

---

[1] Circular states of atomic and molecular systems are an important subject. They have been extensively studied both theoretically and experimentally for several reasons (see, e.g., [12–15,17,27–40] and references therein): (a) they have long radiative lifetimes and highly anisotropic collision cross sections, thereby enabling experiments on inhibited spontaneous emission and cold Rydberg gases, (b) these classical states correspond to quantal coherent states, objects of fundamental importance, (c) a classical description of these states is the primary term in the quantal method based on the $1/n$-expansion, and (d) they can be used in developing atom chips.

$$\ell = v^2 \sqrt{\frac{(w^2+v^2)^2 + 3\left(w^2 - \frac{v^2}{4}\right)\theta^2}{(w^2+v^2)^{7/2}} + b\frac{\left((1-w)^2+v^2\right)^2 + 3\left((1-w)^2 - \frac{v^2}{4}\right)\theta^2}{\left((1-w)^2+v^2\right)^{7/2}}} \tag{9}$$

we obtain the scaled energy of the electron

$$\varepsilon = \frac{1}{\sqrt{w^2+v^2}} + \frac{b}{\sqrt{(1-w)^2+v^2}} - \frac{\ell^2}{2v^2}$$
$$+ \frac{2w^2-v^2}{(w^2+v^2)^{5/2}}\frac{\theta^2}{4} + b\frac{2(1-w)^2-v^2}{\left((1-w)^2+v^2\right)^{5/2}}\frac{\theta^2}{4}. \tag{8}$$

We can seek the equilibrium points in the (w,v)-plane by finding the two partial derivatives of ε with respect to w and v and setting them equal to zero. The second equation gives the equilibrium value of the scaled angular momentum

See equation (9) above.

and the first equation gives the equilibrium value of v

$$w\frac{(w^2+v^2)^2 + \frac{3}{2}\left(w^2 - \frac{3}{2}v^2\right)\theta^2}{(w^2+v^2)^{7/2}} = b(1-w)$$
$$\times \frac{\left((1-w)^2+v^2\right)^2 + \frac{3}{2}\left((1-w)^2 - \frac{3}{2}v^2\right)\theta^2}{\left((1-w)^2+v^2\right)^{7/2}}. \tag{10}$$

Figure 1 shows the equilibrium plot in the (w,v)-plane for $b = 3$ and $\theta = 0.1$. We see that in addition to the properties described in [13] there is a multivalued range in the neighborhood of $w = 0$ and $w = 1$ which increases as θ increases.

If we scale the internuclear distance R as $r = (Z/L^2)R$, and given $\varepsilon = -(R/Z)E$ from (7), then $E = -(Z/L)^2\varepsilon_1$, where $\varepsilon_1 = \varepsilon/r$ is the scaled energy whose scaling includes only Z and L. From (7), $\ell^2 = L^2/(ZR)$, so this yields $r = 1/\ell^2$, with ℓ taken from (9), giving us the expression for $r(w,v,b,\theta)$. Then we substitute the value of ℓ from (9) into (8) and obtain $\varepsilon(w,v,b,\theta)$, which we divide by $r = 1/\ell^2$, with ℓ again taken from (9), obtaining $\varepsilon_1(w,v,b,\theta)$, whose explicit form is

See equation (11) next page.

Then, solving (10) numerically for v and substituting it into (11) and into $r(w,v,b,\theta)$ we obtain, for the given value of b and θ, the parametric dependence $\varepsilon_1(r)$ representing the scaled energy terms, with the parameter w running over the allowed range determined by (10). The asymptote w_3, corresponding to $v \to \infty$, is the same as in the case of $\theta = 0$, and is equal to $b/(b+1)$, and other limits on w can be determined numerically.

Figures 2 and 3 show the scaled energy terms for the values of the scaled amplitude of the laser field for $\theta = 0.01$ and $\theta = 0.1$ against the unperturbed energy terms for $\theta = 0$. It is seen that for small values of θ the
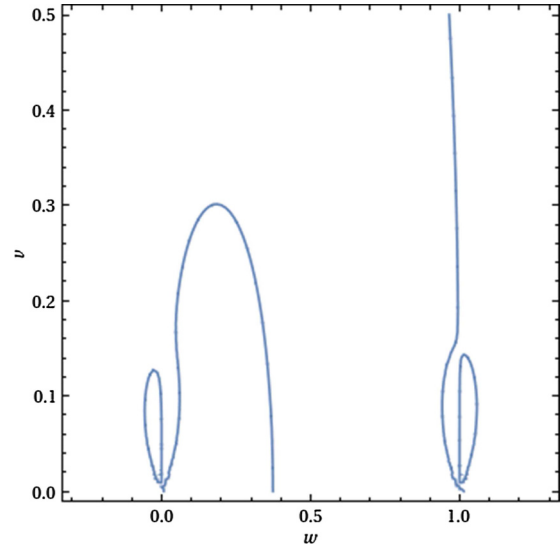

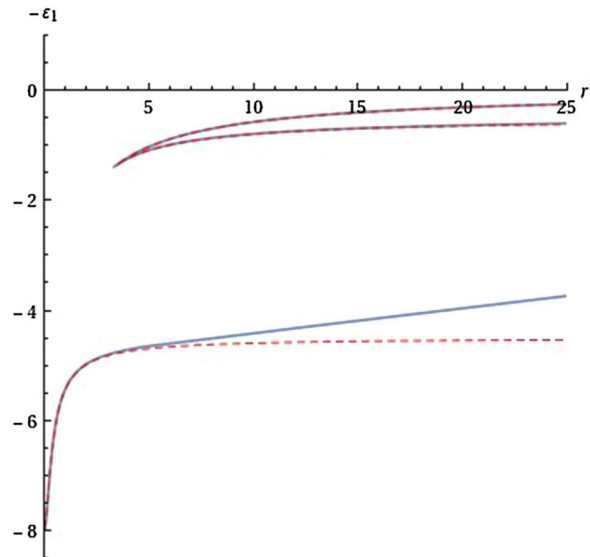**Fig. 1.** Equilibrium plot in the (w,v)-plane for $b = 3$ and $\theta = 0.1$.

Fig. 2. The plot of the scaled energy terms $-\varepsilon_1(r)$ (with r on the horizontal axis and ε_1 on the vertical) for the scaled amplitude of the laser field $\theta = 0.01$ with $b = 3$ shown in blue solid curves against the terms for $\theta = 0$ with $b = 3$ shown in red dashed curves.

lower term is the first affected, and the terms take on a more complex form as θ further increases. We plot $-\varepsilon_1$ on the vertical axis for it to have the same sign as E.

It is seen that as the scaled amplitude θ of the laser field increases the scaled energy terms $\varepsilon_1(r)$ become more and more complex. In particular, at some ranges of θ, the number of the scaled energy terms increases from 3 (which was the case for $\theta = 0$) to 4 or even 5.

$$\varepsilon_1 = v^4 \left(\frac{\left(w^2 + v^2\right)^2 \left(w^2 + \frac{v^2}{2}\right) + \left(w^4 - \frac{5}{2}w^2 v^2 + \frac{v^4}{4}\right) \frac{\theta^2}{2}}{\left(w^2 + v^2\right)^{7/2}} \right.$$

$$+ b \frac{\left((1-w)^2 + v^2\right)^2 \left((1-w)^2 + \frac{v^2}{2}\right) + \left((1-w)^4 - \frac{5}{2}(1-w)^2 v^2 + \frac{v^4}{4}\right) \frac{\theta^2}{2}}{\left((1-w)^2 + v^2\right)^{7/2}} \right)$$

$$\times \left(\frac{\left(w^2 + v^2\right)^2 + 3\left(w^2 - \frac{v^2}{4}\right)\theta^2}{\left(w^2 + v^2\right)^{7/2}} + b \frac{\left((1-w)^2 + v^2\right)^2 + 3\left((1-w)^2 - \frac{v^2}{4}\right)\theta^2}{\left((1-w)^2 + v^2\right)^{7/2}} \right) \quad (11)$$
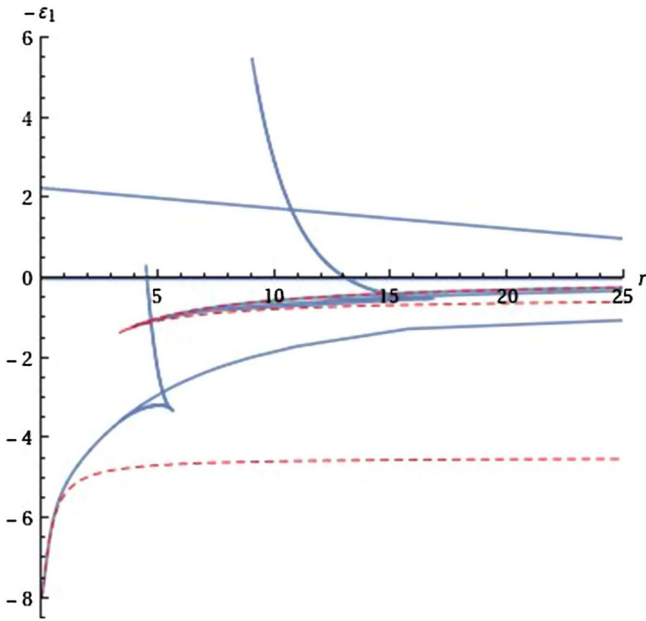

Fig. 3. The plot of the scaled energy terms $-\varepsilon_1(r)$ (with r on the horizontal axis and ε_1 on the vertical) for the scaled amplitude of the laser field $\theta = 0.01$ with $b = 3$, shown in blue solid curves against the terms for $\theta = 0$, with $b = 3$, shown in red dashed curves.

At this point it might be useful to clarify the relation between the classical energy terms $\varepsilon_1(r)$ and the energy E. The former is a scaled quantity related to the energy as specified above in the 1st line after equation (10): $E = -(Z/L)^2 \varepsilon_1$. The projection L of the angular momentum on the internuclear axis is a *continuous* variable. The energy E depends on both ε_1 and L. Therefore, while the scaled quantity ε_1 takes a *discrete* set of values, the energy E takes a *continuous* set of values (as it should be in classical physics).

We also studied the shift of the radiation frequency caused by a high-frequency linearly-polarized laser field The angular momentum of the electron can be expressed as

$$L = \rho^2 \frac{d\varphi}{dt} = \Omega \rho^2 \quad (12)$$

where Ω is the frequency of the motion of the electron. Using the scaled quantities from (7), we have
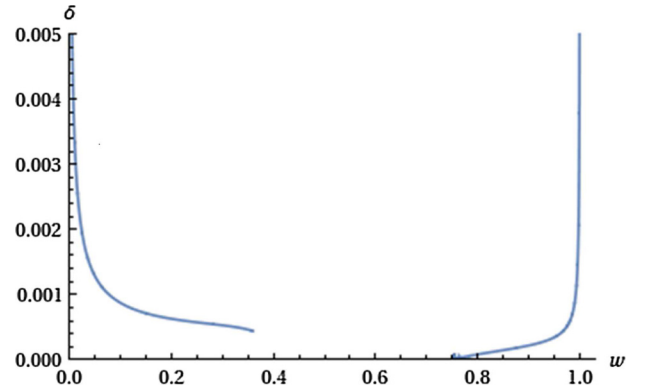

Fig. 4. The relative blue shift of the radiation frequency of the electron versus its scaled axial coordinate for $b = 3$ and $\theta = 0.01$.

$$\Omega = \sqrt{\frac{Z}{R^3}} \tilde{\Omega}, \tilde{\Omega} = \frac{\ell}{v^2} \quad (13)$$

where the tilde above denotes the scaled frequency. The relative shift of the frequency is determined by

$$\delta = \frac{\Omega - \Omega_0}{\Omega_0} = \frac{\Omega}{\Omega_0} - 1 = \frac{\tilde{\Omega}}{\tilde{\Omega}_0} - 1 = \frac{\ell}{\ell_0} \frac{v_0^2}{v^2} - 1 \quad (14)$$

where the subscript index "0" refers to the default case ($\theta = 0$) and the value of v is taken to be the equilibrium value (determined by (10)).

Figures 4 and 5 show the plot of the relative shift of the frequency for the ratio of the nuclear charges $b = 3$ and the values of $\theta = 0.01$ and $\theta = 0.1$. As we can see the shift increases when θ increases, and it is the smallest around the point $w = w_3 = b/(b+1)$.

Thus, for a known amplitude of the laser field, by measuring the relative shift of the radiation frequency it should be possible to determine experimentally the distance of the orbital plane of the electron from the nucleus of the smaller nuclear charge.

2.2 Circular polarization

Now we consider the same configuration subjected to a circularly-polarized laser field of amplitude F and frequency ω, the polarization plane being perpendicular to
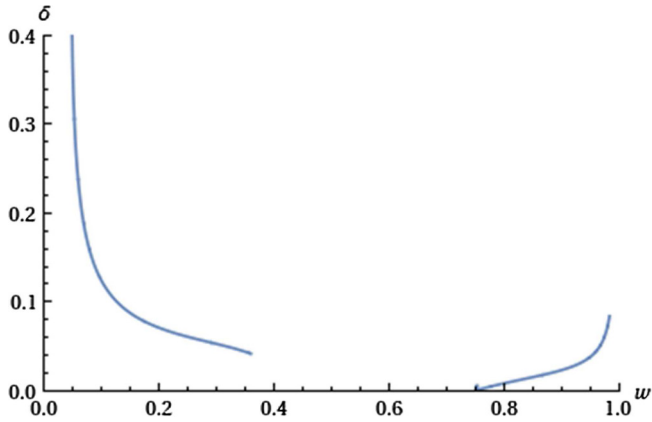
Fig. 5. The relative blue shift of the radiation frequency of the electron versus its scaled axial coordinate for $b = 3$ and $\theta = 0.1$.

the internuclear axis. The laser field varies as

$$\mathbf{F} = F \left(\mathbf{e_x} \cos \omega t + \mathbf{e_y} \sin \omega t \right) \qquad (15)$$

where $\mathbf{e_x}$ and $\mathbf{e_y}$ are the unit vectors along the x- and y-axes (which are perpendicular to the z-axis). In this case the Hamiltonian takes the form

$$H = H_0 + F\rho \cos\left(\varphi - \omega t\right) = H_0 + F\rho \left(\cos\varphi \cos\omega t + \sin\varphi \sin\omega t\right) \qquad (16)$$

where H_0 is given by (1). We denote $V = F\rho \cos\varphi$, $W = F\rho \sin\varphi$ and use the formalism of effective potentials for the circular-polarization case [23,24]:

$$U_0 = \frac{1}{4\omega^2} \left([V, [V, H_0]] + [W, [W, H_0]] \right) = \frac{F^2}{4\omega^2} \qquad (17)$$

$$U_1 = \frac{1}{4\omega^4} \left([[V, H_0], [[V, H_0], H_0]] + [[W, H_0], [[W, H_0], H_0]] \right)$$
$$+ \frac{-1}{2\omega^3} [[V, H_0], [W, H_0]]. \qquad (18)$$

The zeroth-order effective potential in (17) is coordinate-independent and thus does not affect the dynamics of the system. In (18) the last term vanishes and the first-order effective potential is

$$U_1 = \frac{F^2}{4\omega^4} \left(\frac{3L^2}{\rho^4} + Z \frac{z^2 - 2\rho^2}{(z^2 + \rho^2)^{5/2}} + Z' \frac{(R-z)^2 - 2\rho^2}{\left((R-z)^2 + \rho^2\right)^{5/2}} \right). \qquad (19)$$

Repeating the procedure used for the linear-polarization case and using the scaled quantities in (7) we obtain the scaled energy of the electron

$$\varepsilon = \frac{1}{\sqrt{w^2 + v^2}} + \frac{b}{\sqrt{(1-w)^2 + v^2}} - \frac{\ell^2}{2v^2} - \frac{w^2 - 2v^2}{(w^2+v^2)^{5/2}} \frac{\theta^2}{4}$$
$$- b \frac{(1-w)^2 - 2v^2}{\left((1-w)^2 + v^2\right)^{5/2}} \frac{\theta^2}{4} - \frac{3\ell^2}{v^4} \frac{\theta^2}{4}. \qquad (20)$$

We seek the equilibrium points by finding the two partial derivatives of ε with respect to w and v and setting
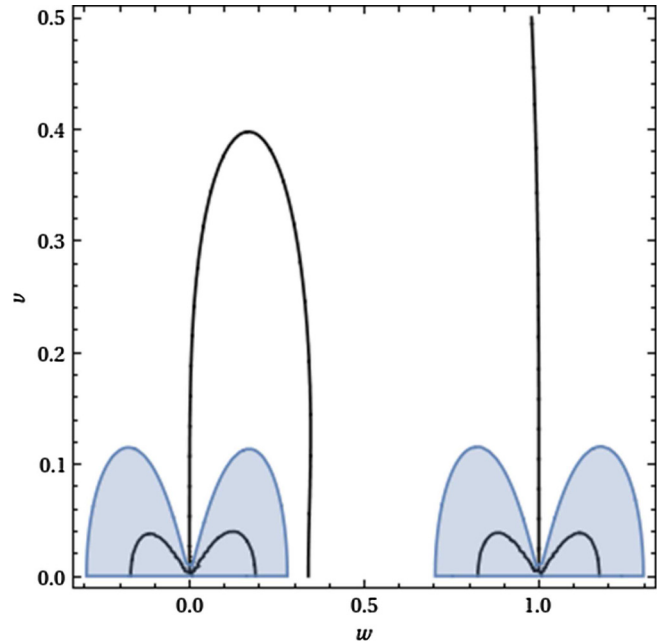

Fig. 6. Equilibrium plot in the (w, v)-plane for $b = 3$ and $\theta = 0.2$. The forbidden region, corresponding to the points where $\ell^2 < 0$, is shaded.

them equal to zero. From the second equation we get the equilibrium value of the scaled angular momentum

See equation (21) *next page.*

and from the first equation we obtain numerically the equilibrium value of v:

$$w \frac{\left(w^2 + v^2\right)^2 - 3\left(\frac{w^2}{4} - v^2\right)\theta^2}{(w^2 + v^2)^{7/2}} = b\,(1 - w)$$
$$\times \frac{\left((1-w)^2 + v^2\right)^2 - 3\left(\frac{(1-w)^2}{4} - v^2\right)\theta^2}{\left((1-w)^2 + v^2\right)^{7/2}}. \qquad (22)$$

We can notice from (21) that ℓ^2 is not strictly non-negative for arbitrary w, v, b and θ (unlike in the case $\theta = 0$, when it is always non-negative), which imposes additional constraint on the validity range in the (w, v)- plane. Figure 6 shows the equilibrium curve in the (w, v)- plane for $\theta = 0.2$ with the forbidden region, where $\ell^2 < 0$, which is shaded. We see that the additional (w, v)-curves due to non-zero θ are entirely within the forbidden region and are therefore discounted from the solution. (In the case of linear polarization, the forbidden region due to ℓ is small, for $b = 3$, $\theta = 0.1$ it doesn't exist – it appears at greater θ, and it does not cover the curves appearing due to non-zero θ).

The properties of the equilibrium curves are as follows. As θ increases from 0, the point w_1, of the intersection of the right branch of the left (w, v)-curve with the abscissa, which is equal to $1/(1 + b^{1/2})$ for $\theta = 0$, displaces to the left, given by the expression

$$w_1 = \frac{1}{1 + \sqrt{\alpha}} \qquad (23)$$

$$\ell = \frac{v^3}{\sqrt{v^2 + 3\theta^2}} \sqrt{\frac{(w^2 + v^2)^2 - \frac{3}{4}(3w^2 - 2v^2)\theta^2}{(w^2 + v^2)^{7/2}} + b\frac{((1-w)^2 + v^2)^2 - \frac{3}{4}(3(1-w)^2 - 2v^2)\theta^2}{((1-w)^2 + v^2)^{7/2}}} \qquad (21)$$
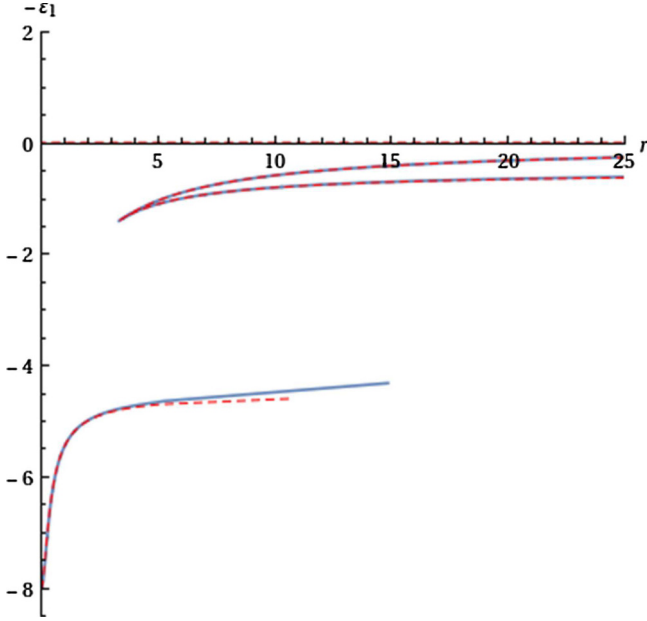

Fig. 7. The plot of the scaled energy terms $-\varepsilon_1(r)$ (with r on the horizontal axis and ε_1 on the vertical) for the scaled amplitude of the laser field $\theta = 0.01$ in the case of circular polarization with $b = 3$ shown in blue, solid curves against the terms for $\theta = 0$ with $b = 3$ shown in red dashed curves.

Fig. 8. The plot of the scaled energy terms $-\varepsilon_1(r)$ (with r on the horizontal axis and ε_1 on the vertical) for the scaled amplitude of the laser field $\theta = 0.3$ in the case of circular polarization, with $b = 3$, shown in blue, solid curves, against the terms for $\theta = 0$, with $b = 3$, shown in red dashed curves.

where α is a solution of $4\alpha(b - \alpha) = 3(1 + \alpha)(b - \alpha)^2\theta^2$, which is given in the Appendix A. We can see from (23) that for $\theta = 0$, $w_1 = 1/(1 + b^{1/2})$, as in [13]. After θ reaches the critical value

$$\theta_c = \sqrt{\frac{4\alpha_c(b - \alpha_c^2)}{15(1 + \sqrt{\alpha_c})^2(b - \alpha_c^3)}} \qquad (24)$$

where α_c is a solution of $(b - \alpha_c^2)^2 = 5(b - \alpha_c)(b - \alpha_c^3)$, ($\alpha_c$ being given in the Appendix A), a small two-valued region appears to the right of w_1 (the situation that we observe in Fig. 5). As θ increases further and reaches the value

$$\theta_{10} = \sqrt{\frac{4\beta^2(b - \beta^2)}{3(1 + \beta)^2(b - \beta^4)}} \qquad (25)$$

where β is a solution of $\frac{b + \beta^3}{b - \beta^2} = 3\frac{b + \beta^5}{b - \beta^4}$, the branch intersects with the forbidden region at $w_{10} = 1/(1 + \beta)$ and, as θ increases further, part of the branch is within the forbidden region, below their intersection. As an example, for the case of $b = 3$, $\theta_c \approx 0.163$ and $\theta_{10} \approx 0.234$. As for the right w-range, it does not depend on θ and is $b/(b + 1) < w < 1$, as in the case of $\theta = 0$ [13].

With the master equations (20)–(22), we proceed as in the linear case: defining $r = 1/\ell^2$ and $\varepsilon_1 = \varepsilon/r$ and
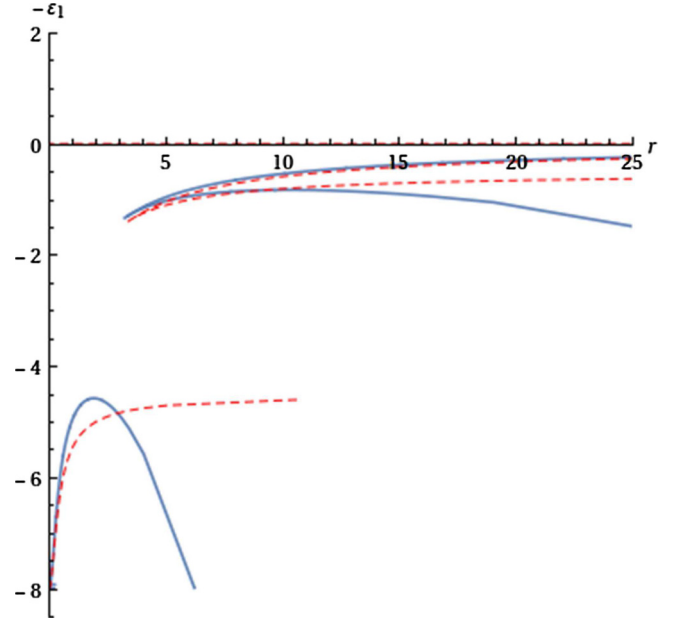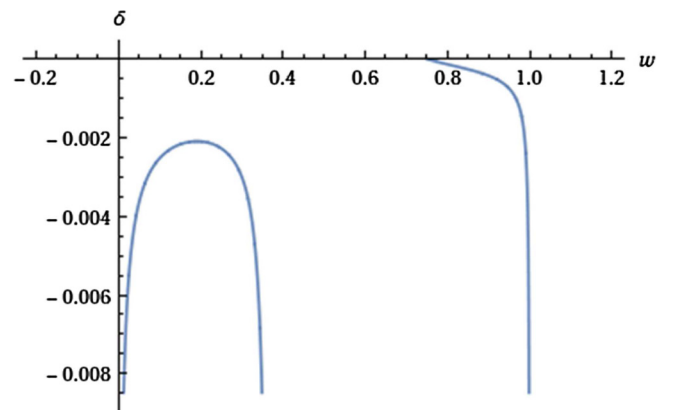

Fig. 9. The relative red shift of the radiation frequency of the electron versus its scaled axial coordinate for $b = 3$ and $\theta = 0.01$ in the case of circular polarization.

numerically solving (22) for v and then substituting it into r and ε_1, we obtain the parametric dependence $\varepsilon_1(r)$ representing the scaled energy terms, with the parameter w running over the allowed range determined by $0 < w < w_1$, $b/(b + 1) < w < 1$ (for $\theta < \theta_c$; for $\theta_c < \theta < \theta_{10}$, w_1 is changed into the point with the maximum w on the left branch, determined numerically, and
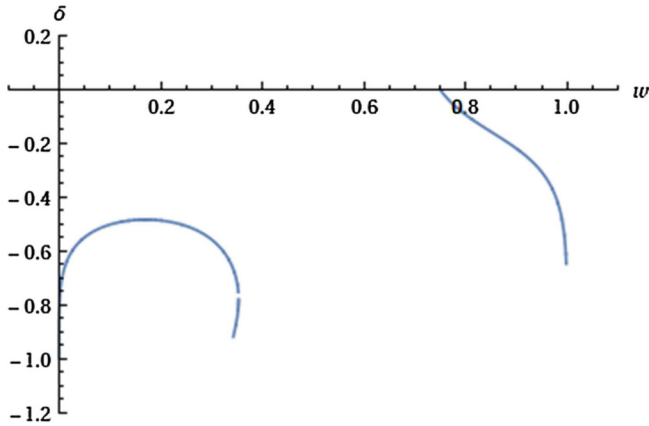
Fig. 10. The relative red shift of the radiation frequency of the electron versus its scaled axial coordinate for $b = 3$ and $\theta = 0.3$ in the case of circular polarization.

for $\theta > \theta_{10}$, it is changed into the point of intersection of the branch with the forbidden region, except when its w-coordinate is less than the maximum w for the branch.

Figures 7 and 8 show the scaled energy terms for the values of the scaled amplitude of the laser field for $\theta = 0.01$ and $\theta = 0.3$ against the unperturbed energy terms for $\theta = 0$. It is seen that for small values of θ the lower term is the first affected, as in the case of linear polarization, and as θ further increases, the terms deviate from the unperturbed ones more, but new terms do not appear.

As in the case of linear polarization, we studied the shift of the radiation frequency caused by a high-frequency circularly-polarized laser field. Following the same procedure to derive the formula for the shift as in the linear-polarization case and using the result in (14), we plot the relative shift of the frequency in Figures 9 and 10. It is seen that in the case of circular polarization, red shift is observed ($\delta < 0$) – the effect opposite to that in the case of linear polarization, where blue shift was observed ($\delta > 0$).

3 Conclusions

We considered the situation where one-electron Rydberg quasimolecules (OERQ) are subjected to a linearly-polarized and circularly-polarized laser field whose frequency is much greater than the highest frequency of the unperturbed system. For obtaining analytical results we used a generalization of the method of effective potentials. We found out that in the case of the linearly-polarized laser field, as the amplitude of the laser field increases, the structure of the energy terms becomes more and more complex. Moreover, the number of the energy terms increases. In the case of the circularly-polarized laser field, new terms do not appear.

We also calculated analytically the shift of the radiation frequency of OERQ caused by the laser field. In both cases, as the amplitude of the laser field increases so does the shift. The radiation frequency of the electron is shifted to the blue in the case of the linearly-polarized laser field, and to the red in the case of circularly-polarized laser field. For a known amplitude of the laser field, by measuring the relative shift of the radiation frequency it should be possible to determine experimentally the distance of the orbital plane of the electron from the nucleus of the smaller nuclear charge.

Author contribution statement

Both authors contributed equally.

Publisher's Note The EPJ Publishers remain neutral with regard to jurisdictional claims in published maps and institutional affiliations.

Appendix A: The explicit form of α in equation (23) and α_c in equation (24)

$$\alpha = \frac{\left(-1 + \sqrt{3}i\right)\left(3\theta^2 - 4\right)\left(3\theta^2\left(1 + 3b\right) - 4\right) + q_\alpha\left(8 - 6\theta^2 - \left(1 + \sqrt{3}i\right)q_\alpha\right)}{18q_\alpha\theta^2} \tag{A.1}$$

where

$$q_\alpha = \left(-\left(3\theta^2 - 4\right)^3 + 27b\theta^2\left(9\theta^4 + 12\theta^2 - 8\right) + 9\sqrt{3}\theta^2\right.$$

$$\left.\times\sqrt{-b\left(64b - 192\left(1 + b + b^2\right)\theta^2 + 432\left(1 + b\right)^2\theta^4 - 108\left(b + 3\right)\left(3b + 1\right)\theta^6 + 81\left(b - 1\right)^2\theta^8\right)}\right)^{1/3} \tag{A.2}$$

$$\alpha_c = \frac{1}{48}\left(15b + \sqrt{3b\left(75b - 64\right) + \frac{5808b^2}{k_\alpha} + 48k_\alpha} + \sqrt{6}\sqrt{b\left(75b - 64\right) - \frac{968b^2}{k_\alpha} - 8k_\alpha + \frac{15\sqrt{3}b\left(128 + b\left(25b - 32\right)\right)}{\sqrt{b\left(75b - 64\right) + \frac{1936b^2}{k_\alpha}}} + 16k_\alpha}\right) \tag{A.3}$$

where

$$k_\alpha = b^{2/3}\left(1350 - 1369b + 1350b^2 + 30\sqrt{3}\left(b - 1\right)\sqrt{675 + b\left(675b - 19\right)}\right)^{1/3} \tag{A.4}$$

References

1. J. Von Neumann, E. Wigner, Phys. Z. **30**, 467 (1929)
2. S.S. Gershtein, V.D. Krivchenkov, Sov. Phys. JETP **13**, 1044 (1961)
3. L.I. Ponomarev, T.P. Puzynina, Sov. Phys. JETP **25**, 846 (1967)
4. J.D. Power, Philos. Trans. R. Soc. London **A274**, 663 (1973)
5. I.V. Komarov, L.I. Ponomarev, S.Y. Slavyanov, *Spheroidal and Coulomb Spheroidal Functions* (Nauka, Moscow, 1976) [in Russian]
6. St. Böddeker, H.-J. Kunze, E. Oks, Phys. Rev. Lett. **75**, 4740 (1995)
7. E. Oks, E. Leboucher-Dalimier, Phys. Rev. E **62**, R3067 (2000)
8. E. Oks, E. Leboucher-Dalimier, J. Phys. B **33**, 3795 (2000)
9. E. Leboucher-Dalimier, E. Oks, E. Dufour, P. Sauvan, P. Angelo, R. Schott, A. Poquerusse, Phys. Rev. E **64**, 065401 (2001)
10. E. Leboucher-Dalimier, E. Oks, E. Dufour, P. Angelo, P. Sauvan, R. Schott, A. Poquerusse, Eur. Phys. J. D **20**, 269 (2002)
11. E. Dalimier, E. Oks, O. Renner, R. Schott, J. Phys. B **40**, 909 (2007)
12. E. Oks, Phys. Rev. Lett. **85**, 2084 (2000)
13. E. Oks, J. Phys. B: Atom. Mol. Opt. Phys. **33**, 3319 (2000)
14. E. Oks, Phys. Rev. E **63**, 057401 (2001)
15. M.R. Flannery, E. Oks, Phys. Rev. A **73**, 013405 (2006)
16. N. Kryukov, E. Oks, Int. Rev. At. Mol. Phys. **2**, 57 (2011)
17. N. Kryukov, E. Oks, Can. J. Phys. **90**, 647 (2012)
18. N. Kryukov, E. Oks, Int. Rev. At. Mol. Phys. **3**, 113 (2012)
19. N. Kryukov, E. Oks, J. Phys. B: At. Mol. Opt. Phys. **46**, 245701 (2013)
20. N. Kryukov, E. Oks, Eur. Phys. J. D **68**, 171 (2014)
21. N. Kryukov, E. Oks, Int. Rev. At. Mol. Phys. **4**, 121 (2013)
22. E. Oks, *Breaking Paradigms in Atomic and Molecular Physics* (Singapore, World Scientific, 2015)
23. B.B. Nadezhdin, in *Radiatsionnye i Relativistskie Effekty v Atomakh i Ionakh* (*Radiative and Relativistic Effects in Atoms and Ions*), (Scientific Council of the USSR Academy of Sciences on Spectroscopy, Moscow, 1986), p. 222 [in Russian]
24. E. Oks, *Analytical Advances in Quantum and Celestial Mechanics: Separating Rapid and Slow Subsystems* (IOP Publishing, Bristol, UK, 2019)
25. P.L. Kapitza, Sov. Phys. JETP **21**, 588 (1951)
26. P.L. Kapitza, Usp. Fiz. Nauk **44**, 7 (1951)
27. A.P. Mishra, T. Nandi, B.N. Jagatap, J. Quant. Spectrosc. Rad. Trans. **120**, 114 (2013)
28. M.R. Flannery, E. Oks, Eur. Phys. J. D **47**, 27 (2008)
29. G. Nogues, A. Lupascu, A. Emmert, M. Brune, J.-M. Raimond, S. Haroche, in *Atom Chips*, edited by J. Reichel, V. Vuletic (Wiley-VCH, Weinheim, Germany, 2011), Ch. 10, Sect. 10.3.3
30. J.N. Tan, S.M. Brewer, N.D. Guise, Phys. Scr. **T144**, 014009 (2011)
31. N. Kryukov, E. Oks, Int. Rev. At. Mol. Phys. **3**, 17 (2012)
32. J.S. Dehesa, S. Lopez-Rosa, A. Martinez-Finkelshtein, R.J. Janez, Int. J. Quantum Chem. **110**, 1529 (2010)
33. T. Nandi, J. Phys. B: At. Mol. Opt. Phys. **42**, 125201 (2009)
34. U.D. Jentschura, P.J. Mohr, J.N. Tan, B.J. Wundt, Phys. Rev. Lett. **100**, 160404 (2008)
35. A.V. Shytov, M.I. Katsnelson, L.S. Levitov, Phys. Rev. Lett. **99**, 246802 (2007)
36. M. Devoret, S. Girvin, R. Schoelkopf, Ann. Phys. **16**, 767 (2007)
37. E. Oks, Eur. Phys. J. D **28**, 171 (2004)
38. L. Holmlid, J. Phys.: Condens. Matter **14**, 13469 (2002)
39. S.K. Dutta, D. Feldbaum, A. Walz-Flannigan, J.R. Guest, G. Raithel, Phys. Rev. Lett. **86**, 3993 (2001)
40. H. Carlsen, O. Goscinski, Phys. Rev. A **59**, 1063 (1999)